RSC Advances

PAPER

View Article Online
View Journal | View Issue

Cite this: *RSC Adv.*, 2019, **9**, 14520

Preparation of core–shell structured metal–organic framework@PANI nanocomposite and its electrorheological properties

Qingkun Wen,[a] Lili Ma,[ab] Chengwei Wang,[a] Baoxiang Wang,*[ab] Rongjiang Han,[a] Chuncheng Hao*[ab] and Kezheng Chen[a]

Received 25th March 2019
Accepted 2nd May 2019

DOI: 10.1039/c9ra02268f

rsc.li/rsc-advances

A novel core–shell-type electrorheological (ER) composite material was fabricated *via* using polyaniline as an insulating layer to the outer surface of the core conductive metal–organic framework (MIL-125) with controlled size and morphology. MIL-125 was firstly synthesized by a solvothermal method, and then polyaniline was synthesized in a polar solvent and a tight coating was successfully achieved to form a MIL-125@PANI core–shell nanocomposite. This core–shell structure greatly enhances the polarization ability of dispersed particles, thereby improving their rheological properties. The morphology of pure MIL-125 and MIL-125@PANI has been characterized by transmission electron microscopy (TEM) and scanning electron microscopy (SEM). Their structure was characterized by X-ray powder diffraction. Moreover, the ER activity of MIL-125-based and MIL-125@PANI-based ER fluids by dispersing the particles into silicone oil was studied using a rotational rheometer. The results show that the MIL-125@PANI composite particles have higher ER properties.

1. Introduction

Intelligent fluids are currently receiving widespread attention and they can respond to various environmental stimuli such as temperature, pH, stress, external magnetic or electric field.[1–3] As a typical smart material, electrorheological (ER) fluid is a general term for a class of liquids, which is prepared by dispersing polarizable particles into an insulating medium fluid such as mineral or silicone oil.[4,5] The shear stress of the so-called ER liquid increases significantly with the increase of the electric field strength. When the external electric field increases to a certain value, the rheological properties of the ER fluid will be changed.[6–8] This changed process is very fast, usually within a few milliseconds, and the conversion process is reversible. This means that the rheological properties of the ER fluids vary with the external applied electric field. When the electric field is applied, the solid particles in the ER fluid will form a chain or columnar structure along the direction of the electric field, causing the ER fluid to change from liquid to solid-like. In this case, its rheological properties will be greatly improved, including shear stress, yield stress and storage/loss modulus,[9–12] *etc.* ER fluids have great application prospects in many fields, including brake/clutch, engine mounts, dampers, and medical haptic devices.[13–15]

At present, the research on ER fluids mainly focuses on dispersed phase particles, which generally have a high dielectric constant and/or appropriate conductivity. The dispersed phase particles can be made of inorganic materials, organic polymer materials, and composite materials, *etc.*[16–19] Among them, composite materials generally consist of a core conductive layer and an insulating layer. The core conductive layer can make the particles rapidly polarize under the action of an electric field and can control the density and shape of the particles. The outermost insulating layer is mainly used to reduce the conductivity, protect the polarization charge does not spread, and control the electrostatic interaction between the particles.[20–22] In this way, the rheological properties can be improved.

Metal–organic framework (MOF) materials are periodic porous materials formed by self-assembly of transition metal ions and organic ligands. They are affected in many fields due to their high porosity, low density, and large specific surface area.[23,24] The size and shape of the MOF particles has an important effect on its function. From previous report, the amount of surfactant CTAB can control the morphology of the coordination polymer $[Cu_3(BTC)_2]$, and even reduce the particle size to the nanoscale.[24] However, MOF is not suitable for the direct using as the dispersed phase of ER material. Because MOF has a large conductivity and it is easy to short-circuit or breakdown due to excessive leakage current density under the application of an external electric field.[25–27] In these cases, it may be used as the core conductive layer and compound with an insulating polyaniline on its surface to form an excellent dispersion of ER fluid. We can achieve step-less regulation by

[a]*College of Materials Science and Engineering, Qingdao University of Science and Technology, Qingdao 266042, PR China. E-mail: bxwang@qust.edu.cn; hao@qust.edu.cn; Fax: +86-532-84022509; Tel: +86-532-84022509*

[b]*State Key Laboratory of Power Transmission Equipment & System Security and New Technology, Chongqing University, Chongqing 400044, PR China*

preparing such an ER fluid as a shock absorber, and can effectively prevent resonance. At the same time, when driving on different roads, this kind of electro-variable shock absorber can intelligently and effectively change the shock absorption to adapt to different situations, and this effect is better than the effect of the spring shock absorber.

In this work, we prepared a coordination polymer $Ti_8O_8(OH)_4(BDC)_6$ (MIL-125, a form of the as-called Ti-incorporated MOF) by solvothermal method.[28] MIL-125 is a photosensitive material with three-dimensional pore structure self-assembled from an octameric ring of Ti–O octahedron and phthalic acid.[29] Polyaniline (PANI) is one of the most well-known conductive polymers and it has been widely investigated because of its great advantages, for example, ease of synthesis, low cost, good chemical stability, sensitive response to an electric field, and reversible doping–dedoping process to control the conductivity.[30–32] Then, an outer-layer of polyaniline is compounded on the surface of MIL-125 in a polar solvent (Dimethylformamide, DMF) to form a new composite material: MIL-125@PANI nanocomposite. It has various advantages of the MOF structure and its stability is improved. The conductivity of MIL-125@PANI is greatly reduced due to its combination of a layer of polyaniline. The composite material of this structure has strong polarization ability and its rheological property is improved greatly. The core/shell MIL-125@PANI particles were dispersed in silicone oil to prepare the ER fluid and their rheological properties were measured at electric field strengths ranging from 0 kV mm^{-1} to 3 kV mm^{-1}. We can see that its ER performance has been significantly improved.

2. Experimental section

2.1 Materials

Dimethylformamide (DMF, Laiyang Fine Chemical Factory, China), anhydrous methanol (CH_4O, Tianjin Fuyu Fine Chemical Co. Ltd., Tianjin, China), acetic acid (CH_3COOH, Tianjin Ruijinte Co., Ltd., Tianjin, China), titanium tetrabutoxide (TBT, Beijing Chemicals, Beijing, China), cetyltrimethyl ammonium bromide (CTAB, Tianjin Bodi Chemical Co. Ltd., China), 1,4-benzenedicarboxylic acid (BDC, Sinopharm Chemical Reagent Corporation, Shanghai, China), aniline monomer (Laiyang Fine Chemical Factory, China), ammonium persulfate (APS, ≥98.0% purity, Beijing Chemicals, China) and silicone oil (polydimethylsiloxane, viscosity: 500 cSt, dielectric constant: 2.63–2.73, density ρ: 0.973 g cm^{-3}, Tian Jin Damao limited company, Tianjin, China) were purchased. All materials were used without any treatment.

2.2 The synthesis of MIL-125

MIL-125 is synthesized by a solvothermal method. Firstly, 5 g BDC and 1 g CTAB were added to a mixture of 100 mL DMF and 15 mL anhydrous methanol, and fully stirred until the mixture was completely dissolved. Subsequently, 5 mL acetic acid was added to the above-solution, which is aimed to prevent the hydrolysis of titanium precursor. After stirring for 10 minutes, 3 mL TBT was added to the above-solution and keep stirring for 30 minutes. Finally, the as-obtained solution was transferred into the autoclave and then reacted under 150 °C for 24 hours. After cooling down, the resulting white product was washed with DMF and anhydrous methanol for several times. The final product was dried in an oven at 65 °C for 12 h.

2.3 The synthesis of MIL-125@PANI nanocomposite

The obtained white MIL-125 solid was dispersed into 100 mL DMF solution, and then 2 mL aniline monomer was added into above solution and stirred continually for 3 h under ice bath. After that, 2 g APS was dissolved in a mixture solution of 50 mL DMF and 0.5 mL water. Then, the APS solution was slowly added to the aniline mixture solution and stirred for 30 minutes under ice bath. The resultant solution was centrifuged and washed with ethanol and water to remove the un-reacted aniline monomer. Finally, the MIL-125@PANI particles were dried at 70 °C in a vacuum oven for 12 h.

2.4 The synthesis of ER fluids

The 10 wt% ER fluids were fabricated by dispersing the as-obtained MIL-125@PANI in silicone oil.

2.5 Characterization

The morphology of the fabricated MIL-125@PANI nanocomposite particles were observed by using a field emission scanning electron microscopy (FESEM, JEOL JSM-6700 F) with an accelerating voltage of 20 kV. TEM images were investigated on a JEOL-2100 high-resolution transmission electron microscopes (Hitachi, Ltd., Tokyo, Japan) operating at 200 kV. For the TEM investigation, small amounts of as-obtained sample dispersed in ethanol was performed an ultrasonic treatment for about 5 min and then be dropped onto a copper grid covered by a carbon film. Its structure was analyzed *via* a powder X-ray diffraction (XRD, Rigaku D/MAX-2500/PC) equipped with a rotating anode and a Cu Kα radiation source ($\lambda = 1.5406$ Å), within the range of 2 theta from 4 to 80°. All studies were taken by using the same condition as follow: a scanning rate 5° min^{-1}, a generator voltage of 40 kV and a current of 100 mA.

The rheological properties of pure MIL-125-based and MIL-125@PANI-based ER fluids were, respectively, studied by a rotational rheometer (HAAKE Rheo Stress 6000, Thermo Scientific, Germany) with a parallel plate system (PPER35, the gap between plates was 1.0 mm), and WYZ-020 DC high-voltage generator (voltage: 0–5 kV, current: 0–1 mA), and a temperature controller. The steady flow curves of shear stress–shear rate were measured by the controlled shear rate (CSR) mode within 0.1–500 s^{-1} at room temperature. Before every measurement, the ER suspensions will be pre-sheared for 60 s at 300 s^{-1} and then electric fields were applied. The so-called yield stress can be approximately obtained with the maximum shear stress values at the low shear rate region. In addition, the dielectric properties of the MIL-125-based and MIL-125@PANI-based ER fluid were detected by using a Novolcontrol broad-band dielectric spectroscopy equipment (Novolcontrol Concept 40, Germany). All experiments were carefully performed at 25 °C.

3. Results and discussion

We have studied a series of synthetic methods for MIL-125@PANI core–shell microspheres, as described in Scheme 1. It is synthesized mainly through a two-step process: (1) the core MOF material was synthesized by solvothermal method; (2) control monomer bonding at the interface is occured and then a coating PANI layer was formed *via* an *in situ* chemical oxidation polymerization. When aniline monomer is added to MIL-125 solution, π-electrons of aromatic systems in the MIL-125 and aniline monomer certainly were combined through π–π* stacking, resulting in a non-covalent functionalization of core particles.[33] In addition, the structure of MOF tends to be round, which provides a core for the growth of polyaniline and facilitates the tight connection between materials.

The external morphology of MIL-125 and MIL-125@PANI particles was observed by SEM technique. As shown in Fig. 1(a) and (b), the shape of as-obtained MIL-125 particle is approximately a spherical morphology with an average size of about 200–300 nm. And it has a smooth surface and monodispersed size. In particular, CTAB has recently been used to synthesize MOF particles and it can adjust the morphology and size of the particles.[33,34] It can be seen from Fig. 1(c) and (d) that the morphology of the MIL-125@PANI nanocomposite particles is basically the same as that of the pure MIL-125, but the average size of the MIL-125@PANI nanocomposite particles also increases slightly, which indicates that polyaniline was successfully coated on the outer surface of the MOF structure in a polar solvent.

Core/shell structured MIL-125@PANI particles can be clearly confirmed by TEM images in Fig. 2. From these TEM images, we can see that the core–shell structure is very clear, the synthesized PANI layer surrounding the MIL-125 core. The sizes of MIL-125@PANI particles depicted in the TEM micrographs are monodispersed, which is consistent with the results observed in the SEM images. The thickness of outer polyaniline layer is about 70–90 nm, which greatly improves the stability and rheological properties of the MOF structure.

The XRD patterns of pure MIL-125 and MIL-125@PANI are shown in Fig. 3, respectively. As displayed in Fig. 3, the XRD pattern of pure MIL-125 corresponds well with the previous report about MIL-125. By comparing the characteristic peaks of XRD, we can see that the characteristic peak of MIL-125@PANI is basically the same as that of MIL-125. We believe that the crystal structure of the composites does not change, and the metal–organic framework structure remains good. The metal–organic framework greatly enhances its polarization ability due to its unique structure, which greatly enhances its rheological properties. However, the intensity of the characteristic peaks is reduced after the formation of MIL-125@PANI particles, which can prove that PANI is successfully coated on the MIL-125 to some extent.

The conductivity has a crucial influence on its rheological properties. Normally, the suitable range of electrical conductivity of the ER material is 10^{-8} to 10^{-10} S cm^{-1}, and adjusting the conductivity to this range is beneficial to enhance its ER activity.[35] In addition, in previous reports, Block *et al.* proposed that the ER fluid exhibiting the best ER effect has an electrical conductivity of about 10^{-9} S cm^{-1}, because the strength of interfacial polarization, in this case, can reach a maximum value.[35] We can calculate the conductivity of the ER suspensions by the formula $\sigma = j/E$, where j is the current density through ER suspension, E is the applied electric field strength. Thus, the conductivity of the MIL-125@PANI particles could be studied by the following conductivity equation:[36–38]

$$\sigma = (1 - \varphi)\sigma_f + \varphi\sigma_p \quad (1)$$

where σ is the conductivity of the MIL-125@PANI-based ER fluid, σ_f is the conductivity of pure silicone oil, σ_p is the conductivity of MIL-125@PANI particles, and φ is the volume fraction of MIL-125@PANI particles in the ER fluid.

The conductivity of pure MIL-125 and MIL-125@PANI ER suspensions are shown in Table 1. The conductivity of MIL-125@PANI maintained within the range of 10^{-10} to 10^{-8} S cm^{-1} and it is good for enhancing ER effect. But the pure MIL-125-based ER fluid possess a high conductivity and shown

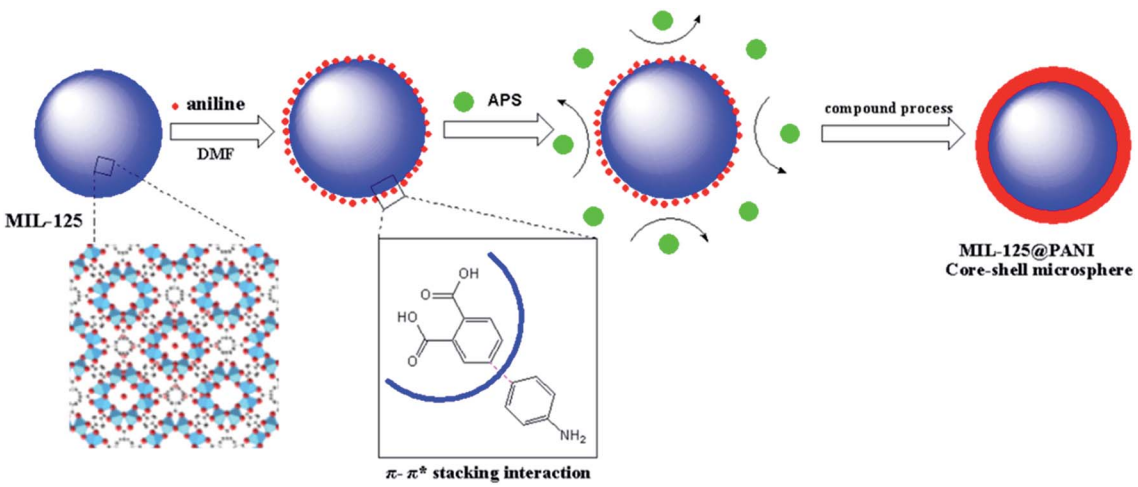

Scheme 1 Schematic diagram of the synthetic process of MIL-125@PANI core–shell type microspheres.

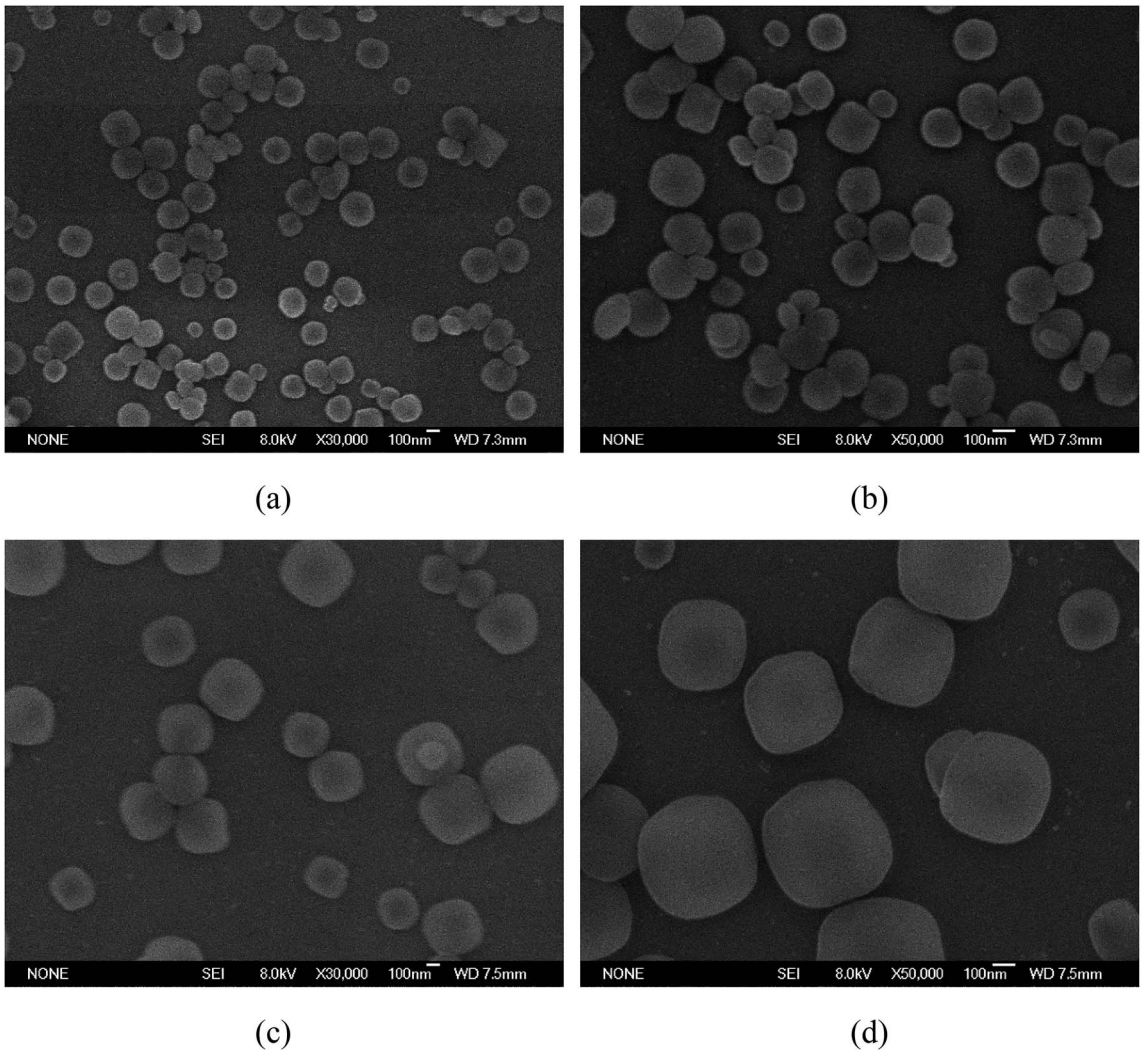

Fig. 1 SEM images of as-synthesized MIL-125 particles (a and b) and MIL-125@PANI particles (c and d).

a break down behavior under $E = 2.5$ kV mm^{-1}. These results verify that the outer polyaniline reduces its conductivity and enhances ER behavior.

The ER characteristics of the MIL-125 and MIL-125@PANI ER suspensions were analyzed in a controlled shear rate (CSR) mode, and it can show the effect of an applied electric field on the flow behavior of ER fluid. The shear rate ranges from 0.1 s^{-1} to 500 s^{-1} and the electric field gradually increases from 0 kV mm^{-1} to 3.0 kV mm^{-1}. The curves of shear stress as a function of the shear rate under different applied electric field are shown in the Fig. 4(a) and (b). When no applied external electric field is occured, the flow characteristics of the ER fluids are the same as those of Newtonian fluid-like behavior, which shear stress increases linearly with increasing shear rate and the slope approaches 1.[39] However, when an electric field is applied, the ER fluids begin to transform toward a "elastic solid", and the shear stress increases as the electric field strength increases, which presents the performance of Bingham fluid-like behavior.[40–44] Because of the formation of the chain-like structure between the dispersed MIL-125@PANI particles, ER fluids exhibited a strong flow resistance. As we can see in Fig. 4(a), as-prepared MIL-125@PANI particles have shown good ER behaviors, a longer plateau region was detected and the shear stress of it can reach more than 200 Pa. We can see that the applied electric field of the pure MIL-125 ER fluid can only reach 2 kV, and continue to increase the voltage will be occurred breakdown (Fig. 4(b)).

As we all know, the properties of ER fluids are mainly due to the chain-like structure or column-like structure formed between the dispersed particles along the direction of electric field. Under the condition of shear flow, the chain-like structure undergoes a process of continuous destruction and recombination. As shown in Fig. 4(a), when the shear rate was low, the shear stress shows a wider plateau region under the application of the electric field. In this process, the chain structure exhibits a dynamic equilibrium between recombination and destruction under the action of electric field strength and shear forces. This is the common feature of the ER fluids. As the electric field strength increases, the electrostatic interaction between the dispersed phase particles increases, resulting in the improvement of the yield stress of the MIL-125@PANI-based ER suspension, which resist the hydrodynamic force. However,

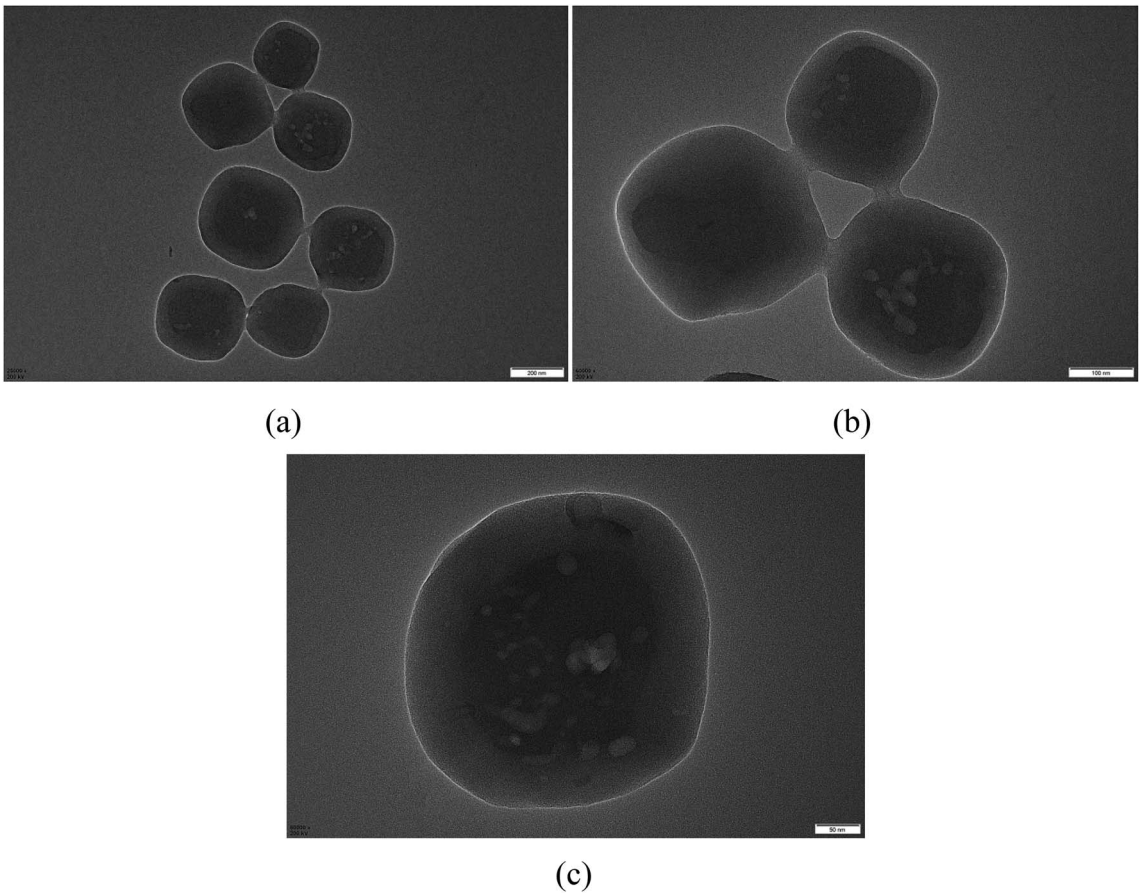

Fig. 2 TEM images of as-synthesized MIL-125@PANI particles.

when the shear rate is increased to a certain extent, the as-called hydrodynamic force becomes dominant because the destruction rate is faster than the recombination rate, which may result a called pseudo-Newtonian fluid behavior.

In addition, Fig. 4(c) and (d) shows the relationship between the shear viscosity and the shear rate of the pure MIL-125 and MIL-125@PANI ER fluid. It was found that the shear viscosity of the pure MIL-125 and MIL-125@PANI ER fluids decrease with the increase of the shear rate, whether the electric field is applied or not, which is called a phenomenon of shear thinning behavior. Moreover, at low shear rate, the shear viscosity of pure MIL-125 and MIL-125@PANI ER fluids increase with the increase of electric field strength. Therefore, the viscosity of MIL-125@PANI-based ER fluid is varied obviously than that of pure MIL-125 ER fluid, and the shear viscosity increases greatly after the electric field is applied, which indicates that ER fluid has a great application prospect in practice.

Furthermore, we usually use ER efficiency to express the performance of ER fluids,[45] as described as follows:

$$e = (\tau_E - \tau_0)/\tau_0 \quad (2)$$

where the τ_0 is indicated as the shear stress without the electric field and the τ_E is the shear stress with various electric field. Through the data in Fig. 4(a), we can calculate that the ER efficiency of above-mentioned MIL-125@PANI-based ER fluid is

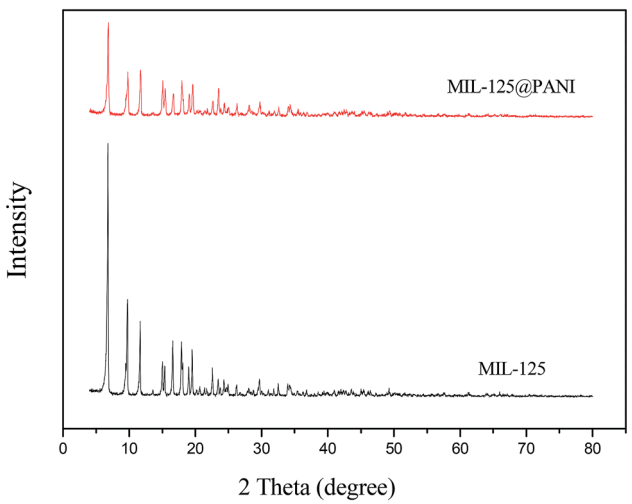

Fig. 3 XRD patterns of pure MIL-125 and MIL-125@PANI particles.

Table 1 The conductivity of pure MIL-125 and MIL-125@PANI

	I/μA	j/μA cm^{-2}	E/kV mm^{-1}	σ/S cm^{-1}	σp/S cm^{-1}
MIL-125	950	192.85	2	$\sim 9.64 \times 10^{-9}$	1.06×10^{-7}
MIL-125@PANI	40	8.12	3	$\sim 2.64 \times 10^{-10}$	$\sim 2.9 \times 10^{-9}$

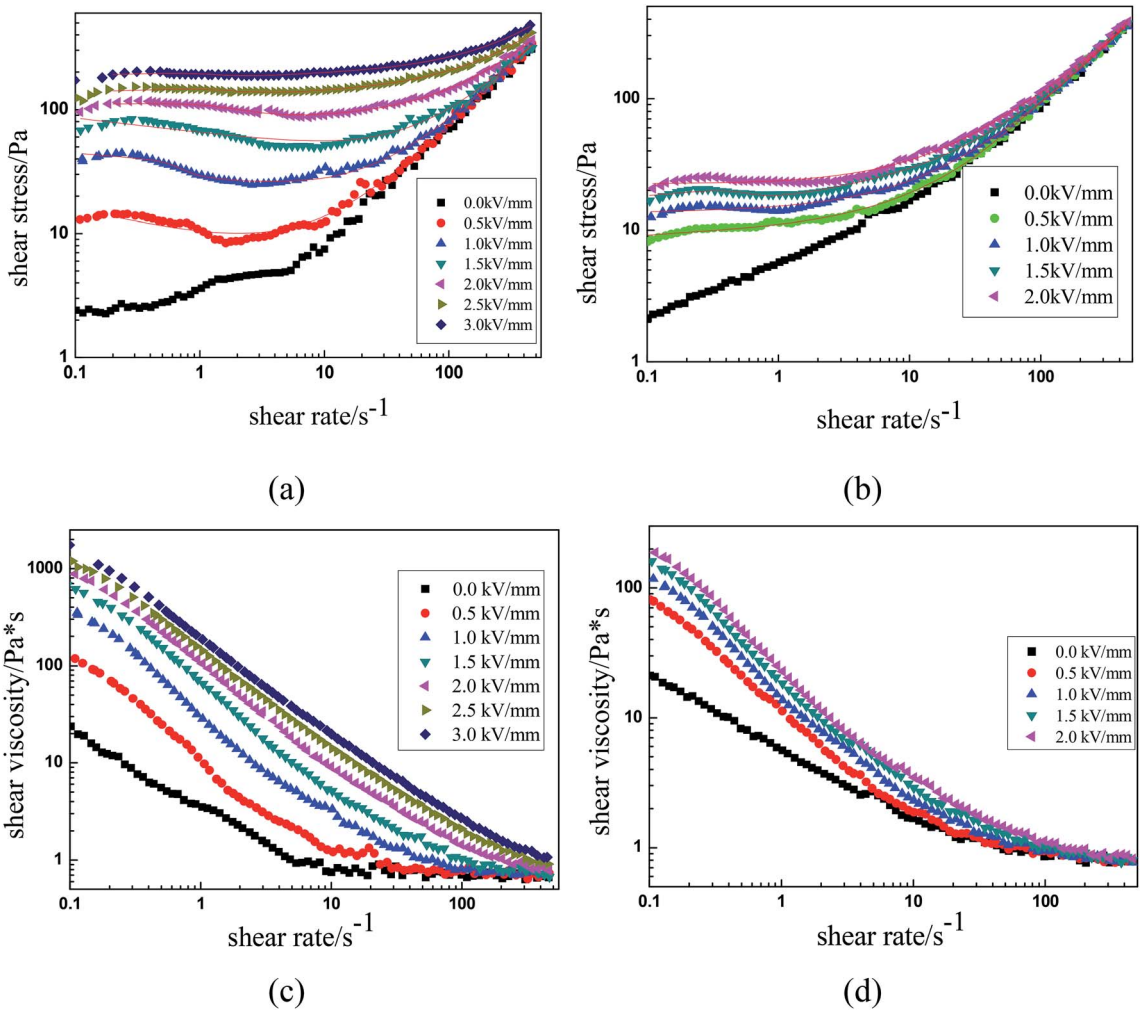

Fig. 4 Shear stress and shear viscosity as functions of shear rate for MIL-125@PANI (a and c) and pure MIL-125 (b and d).

70.86 under the condition of 0.1 s^{-1} shear rate and $E = 3$ kV cm^{-1}.

The Bingham fluid model is usually used to detect the flow curve of ER fluids, which is generally presented as follows:

$$\tau = \tau_0 + \eta\dot{\gamma} \quad \tau \geq \tau_0$$
$$\dot{\gamma} = 0 \quad \tau < \tau_0 \tag{3}$$

where τ and τ_0 represent the shear stress and yield stress, respectively. $\dot{\gamma}$ depict the shear rate, and η is used to describe the shear viscosity. The dynamic yield stress can be calculated by deducing the shear rate to a zero limit. However, the unusual decreasing trend of shear stress–shear rate curves is often occurred, appearing in the Fig. 4(a). Therefore, a called Cho–Choi–Jhon (CCJ) model with six parameters[46] accurately described the best fit of shear stress behavior of the MIL-125@PANI-based ER fluid over the entire range of shear rate under electric field. The equation is shown as below:

Table 2 The optimal parameters in the CCJ model equation obtained from the flow curve shown in Fig. 4a

MIL-125@PANI	Electric field/kV mm^{-1}					
Parameters	0.5	1	1.5	2	2.5	3
τ_0	8.025 ± 0.132	37.504 ± 0.154	70.889 ± 0.338	51.830 ± 0.71	63.705 ± 0.518	75.188 ± 1.228
t_1	0.072 ± 0.02	0.117 ± 0.023	0.233 ± 0.052	0.485 ± 0.082	0.544 ± 0.097	0.783 ± 0.006
α	2 ± 0.063	1.440 ± 0.033	2.006 ± 0.014	2.312 ± 0.078	2.630 ± 0.022	2.77 ± 0.053
β	0.069 ± 0.006	0.069 ± 0.009	0.065 ± 0.015	0.057 ± 0.017	0.053 ± 0.012	0.054 ± 0.017
η_∞	0.198 ± 0.001	0.044 ± 0.0007	0.016 ± 0.0004	0.006 ± 0.0002	0.003 ± 0.0001	0.002 ± 0.015
t_2	1.312 ± 0.021	1.104 ± 0.009	1.118 ± 0.019	0.979 ± 0.011	0.958 ± 0.005	0.96 ± 0.013

Table 3 The optimal parameters in the CCJ model equation obtained from the flow curve shown in Fig. 4b

Pure MIL-125	Electric field/kV mm^{-1}			
Parameters	0.5	1	1.5	2
τ_0	6.518 ± 0.137	13.205 ± 0.96	14.848 ± 0.126	22.387 ± 0.517
t_1	0.015 ± 0.011	0.002 ± 0.009	0.173 ± 0.005	0.007 ± 0.022
α	1.895 ± 0.154	1.805 ± 0.097	4.154 ± 0.088	2.886 ± 0.01
β	0.740 ± 0.035	0.742 ± 0.422	0.732 ± 0.052	0.252 ± 0.007
η_∞	0.061 ± 0.01	0.412 ± 0.0003	0.0286 ± 0.011	0.116 ± 0.006
t_2	0.945 ± 0.036	0.613 ± 0.05	0.889 ± 0.059	0.112 ± 0.041

$$\tau = \frac{\tau_0}{1+(t_1\dot{\gamma})^{\alpha}} + \eta_1\left(1+\frac{1}{(t_2\dot{\gamma})^{\beta}}\right)\dot{\gamma} \quad (4)$$

where τ_0 is described as the dynamic yield stress; η_1 is used for the shear viscosity at the condition of infinite shear rate; t_1 and t_2 represent the time constants, which can be used to depict the variation in the shear stress; the exponent α and β represent the decrease in shear stress at the low shear rate and the increase in shear stress at high shear rate, respectively, and the β has a value range of 0 to 1.[47] Obviously, the CCJ model can better fit the flow curves of MIL-125@PANI-based ER fluid especially at a low shear rate. The six obtained optimal parameter values are both listed in Table 2 and 3. In Fig. 4, a slight reduction occurs firstly at very low shear rates. This probably is due to the time for the application of the electric field is too short, and the rearrangement and arrangement of the particles are not complete. And this hypothesis can be confirmed by Fig. 7 where intermediate values appear before the plateau. Although it is very fast, it takes a certain amount of time to fully reorganize and arrange into a chain structure.

Furthermore, a dynamic oscillation test was carried out to study the visco-elastic behavior of the MIL-125@PANI-based ER fluid, as shown in Fig. 5. The linear viscoelastic region of ER fluid was determined by strain amplitude sweep test with a fixed angular frequency of 6.28 rad s^{-1} within an adequate strain range from 10^{-3} to 10^{2}%. With or without the application of an electric field, both storage modulus (G') and loss modulus (G'') show a plateau region as the strain amplitude increases, and G' and G'' begin to decrease until the strain amplitude reaches 1%. And when an electric field is applied, G' and G'' are increased to higher values, respectively. In this platform area, G' is much larger than G'', which is the so-called linear viscoelastic area (γ_{LVE}), in which the deformation of structure is reversible. When the strain amplitude exceeds γ_{LVE}, both G' and G'' decrease rapidly, and G'' exceeds G', because the irreversible change of the chain structure occurs in the ER fluid, and the chain structure begins to break, resulting in a decrease in the elastic properties of ER fluid.

Moreover, the dynamic yield stress of the MIL-125@PANI-based ER fluid is shown in Fig. 6, the drawing is shown by using log–log coordinates. It can be seen that there is a power-law exponential relationship between the yield stress and the electric field intensity according to the results obtained from

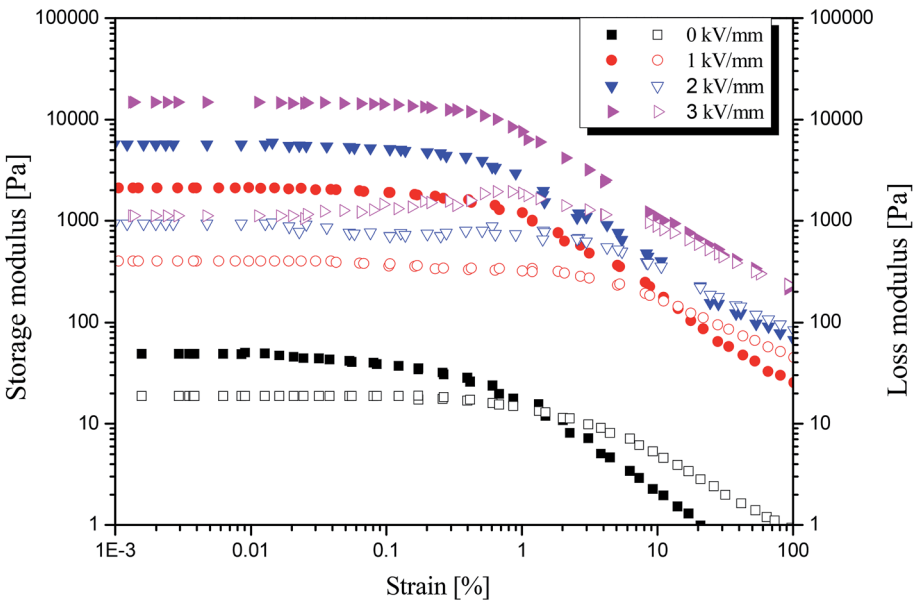

Fig. 5 Storage and loss modulus of MIL-125@PANI-based ER fluid from a strain sweep test.

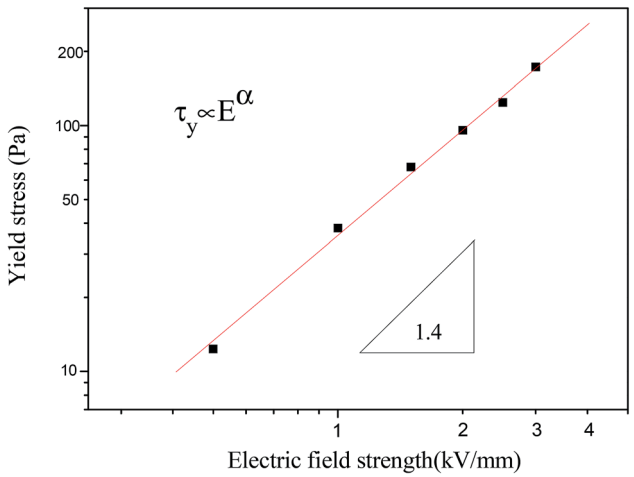

Fig. 6 The yield stress as a function of applied electric field strength for MIL-125@PANI-based ER fluid.

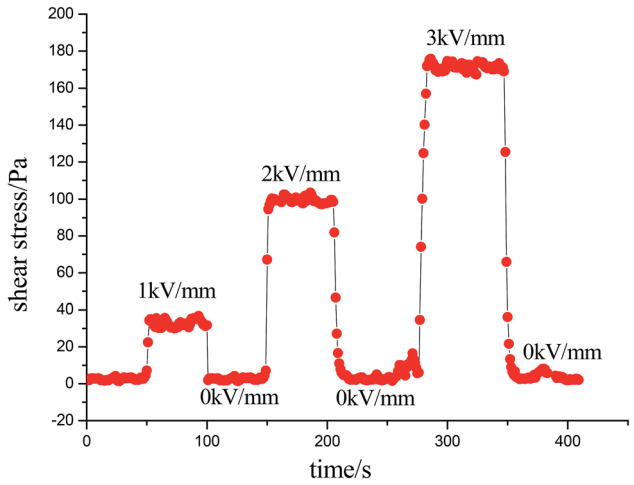

Fig. 7 Shear stress of the MIL-125-based ER fluid influenced by alternating on–off state of electric field at a fixed shear rate of 1 s^{-1}.

the model of controlling the shear rate (CSR model). In general, this relationship can be expressed by the following equation:

$$\tau_y \propto E^{\alpha} \quad (5)$$

where α represents the slope of the line in Fig. 6, and its value varies in a range from 1.0 to 2.0, depending on the ER materials. When the ER fluid is shown a conductivity model, its slope is 1.5. And when the ER fluid is displayed a polarization model, its slope is 2.[48,49] After a linear fitting calculation, the MIL-125@PANI-based ER fluid meets the power-law relationship with an exponent of 1.4, which is very close to the conductivity model. The value of α is related to particle concentration, particle shape, particle composition, temperature and applied electric field strength, *etc.* The slope of the straight line is 1.4, which only shows that it is very close to the conductivity model.

The on–off effect of MIL-125@PANI-based ER fluid is shown in Fig. 7. At a constant shear rate, the sensitivity and reversibility of the MIL-125@PANI-based ER fluid can be observed by periodically turning on and off the applied electric field. Whenever a stable electric field is applied, the shear stress of the MIL-125@PANI-based ER fluid rapidly increases to a certain value, when the applied electric field is removed, the ER fluid will quickly drop to zero electric field value. And the whole process of change is very rapid. This indicates that the response of the MIL-125@PANI-based ER fluid to the electric field strength is very sensitive and reversible.

In general, the intensity of ER performance is also related to the dielectric properties of the material, which can affect the rheological properties by enhancing the polarization between the particles.[50] As reported previously, a proper dielectric loss (ε'') and a large dielectric constant (ε') can improve the activity of ER fluid.[51,52] The relation between the two components of the dielectric constant and the frequency and the Cole–Cole's plot are shown in Fig. 8. The Cole–Cole's equation is usually used to analyze the dielectric spectrum, as described below:

$$\varepsilon^* = \varepsilon' + i\varepsilon'' = \varepsilon_\infty + \frac{\Delta\varepsilon}{(1 + i\omega\lambda)^{1-\alpha}} \quad (6)$$

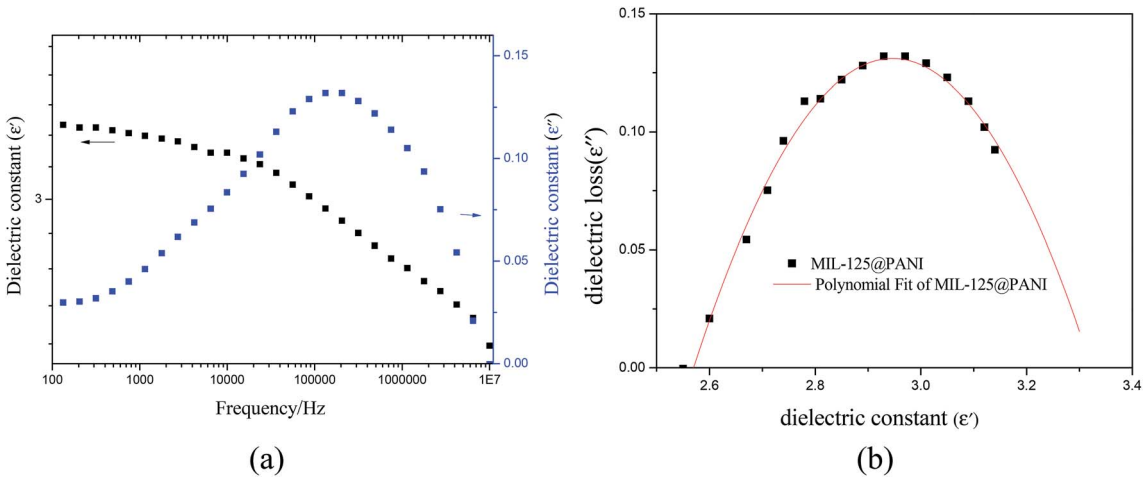

Fig. 8 (a) Dielectric constant and loss factor as a function of the frequency and (b) Cole–Cole plot of MIL-125@PANI ER fluid.

where ε' and ε'' represent the dielectric constant and dielectric loss, respectively; $\Delta\varepsilon'$ ($\Delta\varepsilon' = \varepsilon_0 - \varepsilon_\infty$) is the difference in dielectric constant, it can also be used to describe the strength of polarization among particles of ER fluid under electric field. And ε_0 and ε_∞ is the value of zero frequency and infinite frequency, respectively. The exponent $1 - \alpha$ can indicate the distribution of relaxation time over the entire frequency range. $\lambda = 1/2\pi f_{max}$ (f_{max} is the frequency at which the dielectric loss peaks) is the relaxation time, which represent the polarizability of the particles under an applied electric field. By calculation, the value of the relaxation time λ of the MIL-125@PANI-based ER fluid is 7.76×10^{-7} s. The relaxation time of MIL-125@PANI-based ER fluid is very short, which indicates that it can respond faster to the reorganization of the chain structure and can offset the shear deformation.

4. Conclusion

In summary, we successfully synthesized the core–shell-structured MIL-125@PANI nanocomposite in a polar solvent. SEM and TEM images showed that MIL-125@PANI nanocomposite have a well-defined size distribution with uniform coating layer. Moreover, based on various characterizations, we determined that the as-synthesized MIL-125@PANI could be applied as an ER material and the rheological test showed that the suspension consisting of MIL-125@PANI particles exhibits a strong ER effect. The CCJ model was used to predict the unusual shear stress behavior changed with the applied electric field. A dielectric analysis was performed by measuring the frequency dependence of the dielectric properties for the MIL-125@PANI-based ER fluid, which can better explain the relationship between the particle polarizability and ER effect. The dynamic yield stress showed a power law dependence of the electric field, $\tau_y \propto E^{1.4}$, which is consistent with a conduction model. This result of our study provides a useful method for future intelligence materials preparation.

Conflicts of interest

There are no conflicts to declare.

Acknowledgements

This work was supported by the Shandong Provincial Natural Science Foundation, China (ZR2019MEM051); and Visiting Scholarship of State Key Laboratory of Power Transmission Equipment & System Security and New Technology (Chongqing University, 2007DA10512718401). Training Programs of Innovation and Entrepreneurship for Undergraduates (Qingdao University of Science and Technology, 201810426207).

References

1 D. E. Park, H. S. Chae, H. J. Choi and A. Maity, Magnetite–Polypyrrole Core–Shell Structured Microspheres and Their Dual Stimuli-Response under Electric and Magnetic Fields, *J. Mater. Chem.*, 2015, **3**, 3150–3158.
2 C. Tsitsilianis, Responsive reversible hydrogels from associative "smart" macromolecules, *Soft Matter*, 2010, **6**, 2372–2388.
3 W. Wu, T. Zhou, A. Berliner, P. Banerjee and S. Zhou, Smart Core–Shell Hybrid Nanogels with Ag Nanoparticle Core for Cancer Cell Imaging and Gel Shell for pH-Regulated Drug Delivery, *Chem. Mater.*, 2010, **22**, 1966–1976.
4 J. Yin, X. Xiang, L. Xiang and X. Zhao, Coaxial cable-like polyaniline@titania nanofibers: facile synthesis and low power electrorheological fluid application, *J. Mater. Chem.*, 2010, **20**, 7096–7099.
5 X. Niu, M. Zhang, J. Wu, W. Wen and S. Ping, Generation and manipulation of "smart" droplets, *Soft Matter*, 2009, **5**, 576–581.
6 B. Wang, X. Tian, H. Kai, L. Ma, S. Yu, C. Hao, K. Chen and Q. Lei, Hollow PAQR nanostructure and its smart electrorheological activity, *Polymer*, 2016, **83**, 129–137.
7 S. Dai, P. Ravi and K. Tam, Thermo- and photo-responsive polymeric systems, *Soft Matter*, 2009, **5**, 2513–2533.
8 F. D. Jochum and T. Patrick, Temperature- and light-responsive smart polymer materials, *Chem. Soc. Rev.*, 2013, **42**, 7468–7483.
9 R. Tao, H. Tang, K. Tawhid-Al-Islam, E. Du and J. Kim, Electrorheology leads to healthier and tastier chocolate, *Proc. Natl. Acad. Sci. U. S. A.*, 2016, **113**, 7399–7402.
10 Y. Dong, Y. Liu, J. Yin and X. Zhao, Preparation and enhanced electro-responsive characteristic of graphene/layered double-hydroxide composite dielectric nanoplates, *J. Mater. Chem. C*, 2014, **2**, 10386–10394.
11 H. J. Choi and M. S. Jhon, Electrorheology of Polymers and Nanocomposites, *Soft Matter*, 2009, **5**, 1562–1567.
12 B. Wang, Y. Yin, C. Liu, S. Yu and K. Chen, Synthesis of flower-like $BaTiO_3/Fe_3O_4$ hierarchically structured particles and their electrorheological and magnetic properties, *Dalton Trans.*, 2013, **42**, 10042–10055.
13 M. Sedlaik, M. Mrlik, V. Pavlinek, P. Saha and O. Quadrat, Electrorheological properties of suspensions of hollow globular titanium oxide/polypyrrole particles, *Colloid Polym. Sci.*, 2012, **290**, 41–48.
14 J. Y. Hong and J. Jang, Highly stable, concentrated dispersions of graphene oxide sheets and their electro-responsive characteristics, *Soft Matter*, 2012, **8**, 7348–7350.
15 B. Wang, C. Liu, Y. Yin, S. Yu, K. Chen, P. Liu and B. Liang, Double template assisting synthesized core-shell structured titania/polyaniline nanocomposite and its smart electrorheological response, *Compos. Sci. Technol.*, 2013, **86**, 89–100.
16 S. Chen, X. Huang, W. Wen and P. Sheng, Giant electrorheological effect: a microscopic mechanism, *Phys. Rev. Lett.*, 2010, **105**, 046001.
17 J. Yin, X. Zhao, L. Xiang, X. Xiang and Z. Zhang, Enhanced electrorheology of suspensions containing sea-urchin-like hierarchical Cr-doped titania particles, *Soft Matter*, 2009, **5**, 4687–4697.

18 M. Ken-Ichi, N. Yuki, O. Hiroshi, M. Makoto, S. Wataru and Y. Toshinobu, Synthesis of transparent and field-responsive $BaTiO_3$ particle/organosiloxane hybrid fluid, *Angew. Chem.*, 2010, **49**, 4902–4906.

19 J. W. Kim, F. Liu and H. J. Choi, Polypyrrole/Clay Nanocomposite and its Electrorheological Characteristics, *Ind. Eng. Chem.*, 2002, **8**, 399–403.

20 J. Wu, T. Jin, F. Liu, J. Guo, Y. Cheng and G. Xu, Formamide-modified titanium oxide nanoparticles with high electrorheological activity, *RSC Adv.*, 2014, **4**, 29622–29628.

21 K. He, Q. Wen, C. Wang, B. Wang, S. Yu, C. Hao and K. Chen, A facile synthesis of hierarchical flower-like TiO_2 wrapped with MoS_2 sheets nanostructure for enhanced electrorheological activity, *Chem. Eng. J.*, 2018, **349**, 416–427.

22 T. Plachy, M. Mrlik, Z. Kozakova, P. Suly, M. Sedlacik, V. Pavlinek and I. Kuritka, The electrorheological behavior of suspensions based on molten-salt synthesized lithium titanate nanoparticles and their core-shell titanate/urea analogues, *ACS Appl. Mater. Interfaces*, 2015, **7**, 3725–3731.

23 S. Mendiratta, M. Usman and K. Lu, Expanding the dimensions of metal–organic framework research towards dielectrics, *Coord. Chem. Rev.*, 2018, **360**, 77–91.

24 J. Zhu, P. Z. Li, W. Guo, Y. Zhao and R. Zou, Titanium-based metal–organic frameworks for photocatalytic applications, *Coord. Chem. Rev.*, 2018, **359**, 80–101.

25 Y. D. Liu, J. Kim, W. S. Ahn and H. J. Choi, Novel electrorheological properties of a metal-organic framework $Cu_3(BTC)_2$, *Chem. Commun.*, 2012, **48**, 5635–5637.

26 X. Li, Y. Pi, Q. Hou, H. Yu, Z. Li, Y. Li and J. Xiao, Amorphous TiO_2@NH_2-MIL-125(Ti) homologous MOF-encapsulated heterostructures with enhanced photocatalytic activity, *Chem. Commun.*, 2018, **54**, 1917.

27 X. Shi, Z. Zhang, D. Ke, Y. Lai, F. Jing and L. Jie, Anatase TiO_2@C composites with porous structure as an advanced anode material for Na ion batteries, *J. Power Sources*, 2016, **330**, 1–6.

28 Z. Xiu, M. H. Alfaruqi, J. Gim, J. Song, S. Kim, P. T. Duong, J. P. Baboo, V. Mathew and J. Kim, MOF-derived mesoporous anatase TiO_2 as anode material for lithium–ion batteries with high rate capability and long cycle stability, *J. Alloys Compd.*, 2016, **674**, 174–178.

29 D. H. Meenakshi, S. Christian, F. Théo, R. Laurence, M. Guillaume, S. Clément and F. Gérard, A new photoactive crystalline highly porous titanium(IV) dicarboxylate, *J. Alloys Compd.*, 2010, **131**, 10857–10859.

30 Z. Tian, H. Yu, L. Wang, M. Saleem, F. Ren, P. Ren, Y. Chen, R. Sun, Y. Sun and L. Huang, Recent Progress in the Preparation of Polyaniline Nanostructures and Their Applications in Anticorrosive Coatings, *RSC Adv.*, 2014, **4**, 28195–28208.

31 O. Quatrat and J. Stejskal, Polyaniline in electrorheology, *J. Ind. Eng. Chem.*, 2006, **12**, 352–361.

32 Q. Wen, K. He, C. Wang, B. Wang, S. Yu, C. Hao and K. Chen, Clip-like polyaniline nanofibers synthesized by an insitu chemical oxidative polymerization and its strong electrorheological behavior, *Synth. Met.*, 2018, **239**, 1–12.

33 S. Bao, X. Cai, Y. Shi and M. Pang, Effect of Modulators on Size and Shape-Controlled Growth of Highly Uniform In-NDC-MOF Particles, *CrystEngComm*, 2017, **19**, 1875.

34 X. X. Huang, L. G. Qiu, W. Zhang, Y. P. Yuan, X. Jiang, A. J. Xie, Y. H. Shen and J. F. Zhu, Hierarchically Mesostructured MIL-101 Metal-organic Frameworks: Supramolecular Template-Directed Synthesis and Accelerated Adsorption Kinetics for Dye Removal, *CrystEngComm*, 2012, **14**, 1613.

35 H. Block, J. P. Kelly, A. Qin and T. Watson, Materials and mechanisms in electrorheology, *Langmuir*, 1990, **1**, 12–15.

36 M. Whittle, W. A. Bullough, D. J. Peel, R. Firoozian and R. I. Topics, Dependence of electrorheological response on conductivity and polarization time, *Phys. Rev. E: Stat. Phys., Plasmas, Fluids, Relat. Interdiscip. Top.*, 1994, **49**, 5249.

37 Y. Dong, B. Wang, L. Xiang, Y. Liu, X. Zhao and J. Yin, Influence of Side Chain Sizes on Dielectric and Electrorheological Responses of Poly(ionic liquid)s, *J. Phys. Chem. B*, 2017, **121**, 6226–6237.

38 Y. Liu, J. Yuan, Y. Dong, X. Zhao and J. Yin, Enhanced temperature effect of electrorheological fluid based on cross-linked poly(ionic liquid) particles: rheological and dielectric relaxation studies, *Soft Matter*, 2017, **13**, 1027.

39 M. S. Cho, Y. H. Cho, H. J. Choi and M. S. Jhon, Synthesis and Electrorheological Characteristics of Polyaniline-Coated Poly(methyl methacrylate) Microsphere: Size Effect, *Langmuir*, 2003, **19**, 5875–5881.

40 J. Yin, X. Wang, R. Chang and X. Zhao, Polyaniline decorated graphene sheet suspension with enhanced electrorheology, *Soft Matter*, 2011, **8**, 294–297.

41 W. L. Zhang, Y. D. Liu and H. J. Choi, Graphene oxide coated core–shell structured polystyrene microspheres and their electrorheological characteristics under applied electric field, *J. Mater. Chem.*, 2011, **21**, 6916–6921.

42 Y. D. Liu, B. J. Park, Y. H. Kim and H. J. Choi, Smart monodisperse polystyrene/polyaniline core–shell structured hybrid microspheres fabricated by a controlled releasing technique and their electro-responsive characteristics, *J. Mater. Chem.*, 2011, **21**, 17396.

43 Y. Dong, J. Yin and X. Zhao, Microwave-synthesized poly(ionic liquid) particles: A new material with high electrorheological activity, *J. Mater. Chem. A*, 2014, **2**, 9812–9819.

44 Y. Cao, H. J. Choi, L. Z. Wen, B. Wang, C. Hao and J. Liu, Technology, Eco-friendly mass production of poly(p-phenylenediamine)/graphene oxide nanoplatelet composites and their electrorheological characteristics, *Compos. Sci. Technol.*, 2016, **122**, 36–41.

45 M. Sedlacik, V. Pavlinek, M. Mrlik, Z. Morávková, M. Hajná, M. Trchová and J. Stejskal, Electrorheology of polyaniline, carbonized polyaniline, and their core–shell composites, *Mater. Lett.*, 2013, **101**, 90–92.

46 M. S. Cho, H. J. Choi and M. S. Jhon, Shear stress analysis of a semiconducting polymer based electrorheological fluid system, *Polymer*, 2005, **46**, 11484–11488.

47 S. D. Kim, W. L. Zhang, H. J. Choi, Y. P. Seo and Y. Seo, Electrorheological activity generation by graphene oxide

coating on low-dielectric silica particles, *RSC Adv.*, 2014, **4**, 62644–62650.

48 M. Parthasarathy and D. J. Klingenberg, Electrorheology: Mechanisms and models, *Mater. Sci. Eng.*, 1996, **17**, 57–103.

49 J. Liu, X. Wen, Z. Liu, Y. Tan, S. Yang and P. Zhang, Electrorheological performances of poly(o-toluidine) and p-toluenesulfonic acid doped poly(o-toluidine) suspensions, *Colloid Polym. Sci.*, 2015, **293**, 1391–1400.

50 A. Lengálová, V. R. PavlíNek, P. Sáha, J. Stejskal, T. Kitano and O. Quadrat, The effect of dielectric properties on the electrorheology of suspensions of silica particles coated with polyaniline, *Phys. A*, 2003, **321**, 411–424.

51 S. Lee, J. Lee, S. H. Hwang, J. Yun and J. Jang, Enhanced electroresponsive performance of double-shell SiO_2/TiO_2 hollow nanoparticles, *ACS Nano*, 2015, **9**, 4939–4949.

52 C. M. Yoon, G. Lee, J. Noh, C. Lee, O. J. Cheong and J. Jang, A comparative study of the electrorheological properties of various N-doped nanomaterials using ammonia plasma treatment, *Chem. Commun.*, 2016, **52**, 4808–4811.